ELSEVIER

Int. J. Therm. Sci. 41 (2002) 440–446

International Journal of Thermal Sciences

www.elsevier.com/locate/ijts

Free convection in an enclosure with vertical wavy walls

Shohel Mahmud, Prodip Kumar Das, Nasim Hyder, A.K.M. Sadrul Islam *

Department of Mechanical Engineering, Bangladesh University of Engineering and Technology (BUET), Dhaka 1000, Bangladesh

Received 24 January 2001; accepted 2 August 2001

Abstract

This paper describes a numerical prediction of heat transfer and fluid flow characteristics inside an enclosure bounded by two isothermal wavy walls and two adiabatic straight walls. Governing equations were discretized using the finite-volume method with collocated variable arrangement. Simulation was carried out for a range of wave ratio λ (defined by amplitude/average width) 0.00–0.4, aspect ratio A (defined by height/average width) 1.0–2.0, Grashof number $Gr = 10^0$–10^7 for a fluid having Prandtl number 0.7. Streamlines and isothermal lines are used to present the corresponding flow and thermal field inside the enclosure. Local and global distributions of Nusselt number are presented for the above configuration. Lastly, velocity profiles are presented for some selected locations inside the enclosure for better understanding of the influence of flow field on the thermal field.

Keywords: Finite-volume method; Laminar flow; Natural convection; Wavy wall

1. Introduction

Heat transfer and fluid flow inside wavy-walled enclosures has not been investigated widely due to geometric complexity. Numerous references deal with enclosures with flat walls due to its huge applications in engineering and geophysical systems like solar-collectors, double-wall insulation, electric machinery, cooling system of electronic devices, natural circulation in the atmosphere, the molten core of the Earth etc. These are always complex interactions between the finite fluid content inside the enclosure with the enclosure walls. This complexity increases when the wall becomes wavy or with the change of orientation of the enclosure. Hadjadj and Kyal [1] numerically investigated the effect of sinusoidal protuberances on heat transfer and fluid flow inside an annular space using a non-orthogonal coordinate transformation. They reported that both local and average heat transfer increase with the increase of protuberances amplitude and Grashof number and decreasing Prandtl number. Kumar [2] presented parametric results of flow and thermal field inside a vertical wavy enclosure with porous media. He concluded that the surface temperature was very sensitive to the drifts in the surface undulations, phase of the wavy surface and number of the wave. Yao [3] presented the near wall characteristics of flow and thermal field of a vertical wavy wall. Saidi et al. [4] presented numerical and experimental results of flow over and heat transfer from a sinusoidal cavity. They reported that the total heat exchange between the wavy wall of the cavity and flowing fluid was reduced by the presence of vortex. Vortex plays the role of a thermal screen, which creates a large region of uniform temperature in the bottom of the cavity. Asako and Faghri [5] gave a Finite-Volume prediction of heat transfer and fluid flow characteristics inside a corrugated duct bounded by sinusoidally wavy surface. Lage and Bejan [6] documented heat transfer results near a periodically (timewise and spatial) stretching wall. Hamady et al. [7] and Ozoe et al. [8] presented numerical and experimental results of heat transfer inside rectangular enclosures at different aspect ratios and orientations. This paper presents flow and heat transfer characteristics inside an isothermal-vertical wavy-walled enclosure bounded by two adiabatic straight walls at different Grashof numbers and orientations for some selected waviness of the surface.

2. Mathematical modeling

Considering a two-dimensional laminar natural convection of a Newtonian fluid in a cavity with vertical wavy wall of height H, average width W, amplitude of the wavy wall as shown in Fig. 1. We assumed that the Boussinesq

* Correspondence and reprints.

E-mail addresses: shohel@me.buet.edu (S. Mahmud), prodip@me.buet.edu (P.K. Das), nasim@me.buet.edu (N. Hyder), sadrul@me.buet.edu (A.K.M. Sadrul Islam).

1290-0729/02/$ – see front matter
PII: S1290-0729(02)01336-4

Nomenclature

a	amplitude of the wave	m	
A	aspect ratio $= H/W$		
$\boldsymbol{g}$	gravity vector	$\mathrm{m\cdot s^{-2}}$	
Gr	Grashof number $= g\beta\Delta T W^3/\nu^2$		
H	height of the cavity	m	
h	heat transfer coefficient	$\mathrm{W\cdot m^{-2}\cdot K^{-1}}$	
K	thermal conductivity	$\mathrm{W\cdot m^{-1}\cdot K^{-1}}$	
Nu	Nusselt number		
Pr	Prandtl number $= \nu/\alpha$		
p	pressure	$\mathrm{N\cdot m^{-2}}$	
P	dimensionless pressure		
Ra	Rayleigh number $= Gr \cdot Pr$		
T	temperature	K	
u	velocity component in x-direction	$\mathrm{m\cdot s^{-1}}$	
U	dimensionless velocity component		
v	velocity component in y-direction	$\mathrm{m\cdot s^{-1}}$	
V	dimensionless velocity component		
W	average width of the cavity	m	
x	horizontal coordinate	m	
X	dimensionless horizontal coordinate		
y	vertical coordinate	m	
Y	dimensionless vertical coordinate		

Greek symbols

α	thermal diffusivity	$\mathrm{m^2\cdot s^{-1}}$
β	thermal expansion coefficient	$\mathrm{K^{-1}}$
λ	surface waviness $= a/W$	
ρ	density of the fluid	$\mathrm{kg\cdot m^{-3}}$
ν	kinematic viscosity	$\mathrm{m^2\cdot s^{-1}}$
Θ	dimensionless temperature	

Subscript

av	average value
∞	At ambient condition
C	average value based on cold wall
H	average value based on hot wall
L	local value
W	Value at the wall
0	Reference value
Δ	Difference between two values

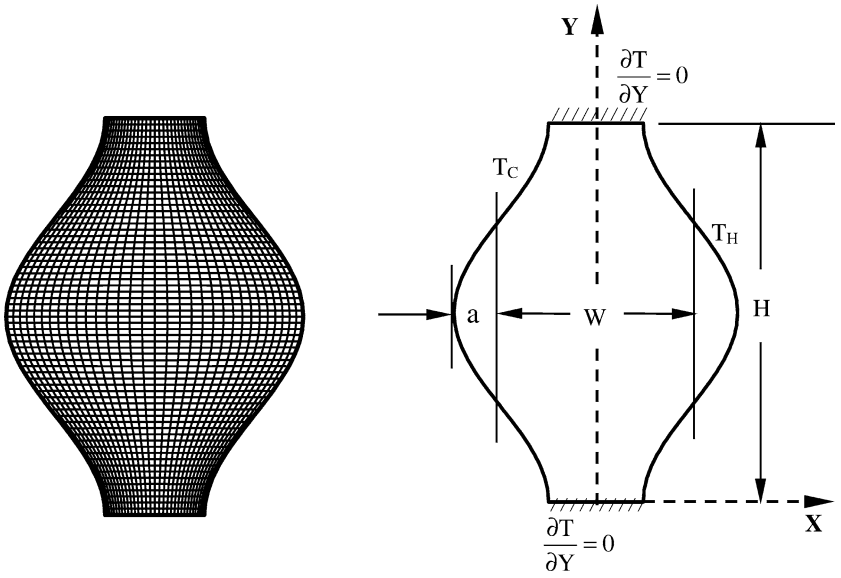

Fig. 1. Schematic diagram of vertical wavy enclosure.

approximation is valid. The governing equations are the continuity equation, Navier–Stokes equations and the energy equation. These equations can be put into dimensionless forms by scaling different lengths with average width W, velocity components with reference velocity V_0 that is equal to $(g\beta\Delta T W)^{1/2}$, pressure with ρV_0^2. The dimensionless temperature can be defined as $\Theta = (T - T_\infty)/\Delta T$ where ΔT is equal to $(T_\mathrm{H} - T_\mathrm{C})$. The governing equations can be written in the following dimensionless form:

$$\frac{\partial U}{\partial X} + \frac{\partial V}{\partial Y} = 0 \tag{1}$$

$$U\frac{\partial U}{\partial X} + V\frac{\partial U}{\partial Y} = -\frac{\partial P}{\partial X} + \frac{1}{\sqrt{Gr}}\left(\frac{\partial^2 U}{\partial X^2} + \frac{\partial^2 U}{\partial Y^2}\right) \tag{2}$$

$$U\frac{\partial V}{\partial X} + V\frac{\partial V}{\partial Y} = -\frac{\partial P}{\partial Y} + \Theta + \frac{1}{\sqrt{Gr}}\left(\frac{\partial^2 V}{\partial X^2} + \frac{\partial^2 V}{\partial Y^2}\right) \tag{3}$$

$$U\frac{\partial \Theta}{\partial X} + V\frac{\partial \Theta}{\partial Y} = \frac{1}{Pr\sqrt{Gr}}\left(\frac{\partial^2 \Theta}{\partial X^2} + \frac{\partial^2 \Theta}{\partial Y^2}\right) \tag{4}$$

2.1. Boundary and initial conditions

Fig. 1 shows the geometry under consideration in the present investigation with different boundary conditions and axis system. The upper and lower walls of the cavity are horizontal and kept adiabatic. The vertical walls are wavy and the surface wave shape is followed by the equations given in Eqs. (7) and (8). Vertical walls are kept isothermal. The wall at the left side is cold ($T = T_C$) and at the right side is hot ($T = T_H$). Initial fluid temperature inside the cavity is T_∞. The initial temperature of the adiabatic walls is equal to the initial fluid temperature T_∞. The gravity acceleration $\boldsymbol{g}$ acts vertically downwards. No slip boundary condition is applied for velocity components at both horizontal and vertical walls. Boundary conditions can be summarized by the following equations:

$$\begin{aligned} &Y = 0, \qquad -\left(\frac{1}{2} - \lambda\right) \leqslant X \leqslant \left(\frac{1}{2} - \lambda\right) \\ &U = V = 0, \qquad \frac{\partial \Theta}{\partial Y} = 0 \end{aligned} \tag{5}$$

$$\begin{aligned} &Y = A, \qquad -\left(\frac{1}{2} - \lambda\right) \leqslant X \leqslant \left(\frac{1}{2} - \lambda\right) \\ &U = V = 0, \qquad \frac{\partial \Theta}{\partial Y} = 0 \end{aligned} \tag{6}$$

$$\begin{aligned} &0 \leqslant Y \leqslant A \\ &X = \left(\frac{1}{2} - \lambda\right) + \lambda\left[1 - \operatorname{Sin}\frac{\pi}{2}\left(1 + \frac{4Y}{A}\right)\right] \\ &U = V = 0, \qquad \Theta = 0 \end{aligned} \tag{7}$$

$$\begin{aligned} &0 \leqslant Y \leqslant A \\ &X = -\left(\frac{1}{2} - \lambda\right) - \lambda\left[1 - \operatorname{Sin}\frac{\pi}{2}\left(1 + \frac{4Y}{A}\right)\right] \\ &U = V = 0, \qquad \Theta = 1 \end{aligned} \tag{8}$$

As the initial condition, a motionless state and uniform temperature are taken:

At $0 < Y < A$.

And

$$\begin{aligned} &-\left(\frac{1}{2} - \lambda\right) - \lambda\left[1 - \operatorname{Sin}\frac{\pi}{2}\left(1 + \frac{4Y}{A}\right)\right] < X \\ &\quad < \left(\frac{1}{2} - \lambda\right) + \lambda\left[1 - \operatorname{Sin}\frac{\pi}{2}\left(1 + \frac{4Y}{A}\right)\right] \\ &U = V = P = \Theta = 0 \end{aligned} \tag{9}$$

2.2. Solution methodology

The numerical technique used in the present study is similar to that of Hortmann et al. [9] based on the finite-volume method as described by Ferziger and Peric [10]. The solution domain is first subdivided into finite number of control volumes (CV). Body fitted, non-orthogonal grids are used. Grids are oriented in such a way that the number of CV is higher near the walls where higher gradients of variable values are expected (see Fig. 1). A collocated variable arrangement is used in the present investigation. All variables are calculated at the center of each CV. SIMPLE algorithm is used. First the momentum equations (Eqs. (2) and (3)) are discretized and linearized. Both the convective and diffusive fluxes are approximated using the CDS scheme, which is second order accurate. Linear interpolation and numerical differentiation [10] are used to express the cell-face value of the variables and their derivatives through the nodal values. Discretized momentum equations lead to an algebraic equation systems for velocity components U and V where pressure, temperature, fluid properties are taken from the previous iteration except the first iteration where initial conditions are applied. These linear equation systems are solved iteratively (inner iteration) to obtain an improved estimate of velocity. The improved velocity field is then used to estimate new mass fluxes, which satisfy the continuity equation. The pressure-correction equation is then solved using the same linear equation solver and to the same tolerance. The energy equation is then solved in the same manner to obtain a better estimate of the new solution. This completes one outer iteration and is repeated until the residual level is less than or equal to 10^{-6}. In this study the SIP-solver based on lower-upper decomposition (ILU) is used to solve the linear equation systems. To avoid divergence, an underrelaxation parameter 0.7 is used for velocity, 0.2 for pressure and 0.9 for temperature.

2.3. Accuracy

In the present investigation a nonorthogonal, nonuniform and nonstaggered grid system is used. Five combinations (10×10, 20×20, 16×32, 32×64, 64×128 and 40×250) of control volumes are used to test the effect of grid size on the accuracy of the predicted results. Fig. 2 shows the

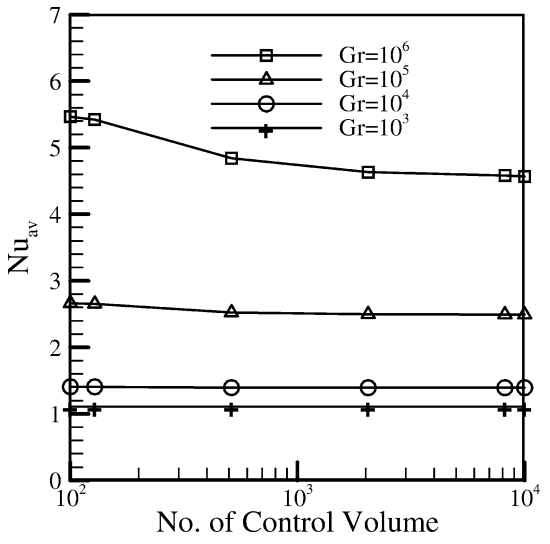

Fig. 2. Average Nusselt number as a function of number of control volume (CV) for $A = 2.0$ and $\lambda = 0.25$.

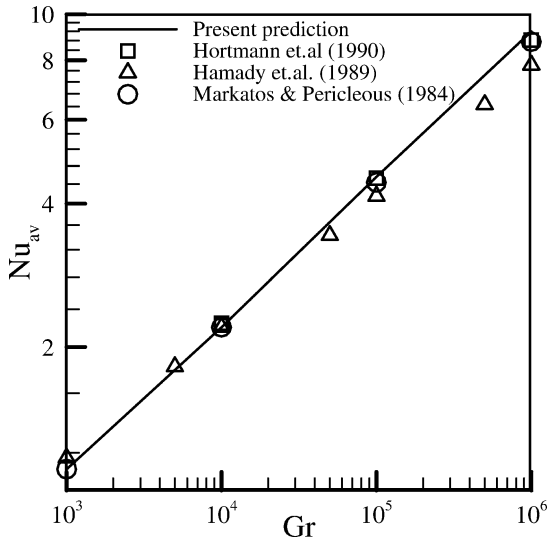

Fig. 3. Validation of average Nusselt number for $A = 1.0$ and $\lambda = 0.0$.

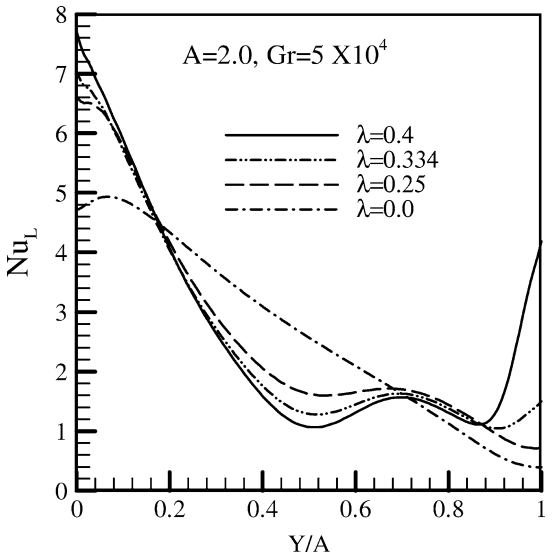

Fig. 4. Local Nusselt number as a function of vertical distance for $A = 2.0$, $Gr = 5 \times 10^4$ and $\lambda = 0.0$–0.4.

distribution of average Nusselt numbers of the hot wall as a function of grid sizes for four different Grashof numbers. It is evident from the figure that for lower Grashof numbers the Nusselt number is independent of the grid sizes studied here and for the higher Grashof numbers the three higher grid sizes (32×64–40×128) give the same result. Thus, throughout this study the results are presented for 64×128 CVs'. Predicted results of average Nusselt numbers for a square cavity ($A = 1, \lambda = 0$) with the same boundary conditions are compared with the benchmark solution of Hortmann et al. [9] and with experimental data of Hamady et al. [7] and Markatos and Pericleous [11]. Fig. 3 shows this comparison. Predicted results show a very good agreement with the reference benchmark solution and experimental works.

3. Results and discussions

3.1. Heat transfer

The local heat transfer is calculated in terms of local Nusselt number using the following equation:

$$Nu_{\mathrm{L}} = \frac{h_{\mathrm{L}} W}{K_{\mathrm{f}}} = \frac{W}{\Delta T}\left(\frac{\mathrm{d}T}{\mathrm{d}x}\right)_W = \left(\frac{\mathrm{d}\Theta}{\mathrm{d}X}\right)_W \tag{10}$$

The local Nusselt number distribution along the hot wavy wall is presented in Fig. 4 for a constant Grashof number ($Gr = 5 \times 10^4$) and four selected surface waviness ($\lambda = 0.4$, 0.334, 0.25, 0.0) for an aspect ratio $A = 2.0$. The heat transfer rate falls along the wavy wall gradually up to the maximum cross-section ($Y/A = 0.5$) of the cavity. Because the temperature gradient normal to the wall falls gradually in vertical direction due to the increase of the cross-section of the cavity up to $Y/A = 0.5$. This nature is similar for each surface waviness with a slight variation in magnitude. In the range $0.5 \leqslant Y/A \leqslant 0.85$, the Nusselt number shows a periodic distribution with respect to the vertical distance. For $Y/A > 0.85$, the Nusselt number strongly depends on the waviness of the vertical wall. For higher waviness ($\lambda = 0.4$) the interwall spacing is very small beyond $Y/A = 0.85$. Convective distortion of the isotherms hardly occur at this portion of the cavity, hence showing higher temperature gradients normal to the wall, as well as local Nusselt numbers. At $\lambda = 0.334$, the pattern is similar as $\lambda = 0.4$, but the Nusselt number is lower. At a moderate surface waviness ($\lambda = 0.25$), the isotherms suffer the convective distortion due to the comparatively higher interwall spacing, hence showing a descending local Nusselt number at this portion of the wall.

Local Nusselt numbers are integrated to calculate the global or average value of Nusselt number according to

$$Nu_{\mathrm{av}} = \frac{1}{H}\int_0^H Nu_{\mathrm{L}}\,\mathrm{d}y \tag{11}$$

the average Nusselt number is plotted as a function of Grashof number in Fig. 5 for an aspect ratio $A = 2.0$ and $\lambda = 0.25$, 0.1666, 0.1 and 0.0. The variation of average Nusselt numbers with Grashof number is independent of the Grashof number, whatever the waviness of the surface below $Gr \approx 10^3$. Up to this Grashof number the heat transfer process is dominated by conduction for all wavy surfaces, like a parallel wall ($\lambda = 0.0$). Beyond this Grashof number ($Gr > 10^3$) the heat transfer increases as the convection dominates, but is less for higher waviness at a particular Grashof number.

3.2. Effect of aspect ratio

Fig. 6 shows the variation of average Nusselt number for a hot wall as a function of the Grashof number for three

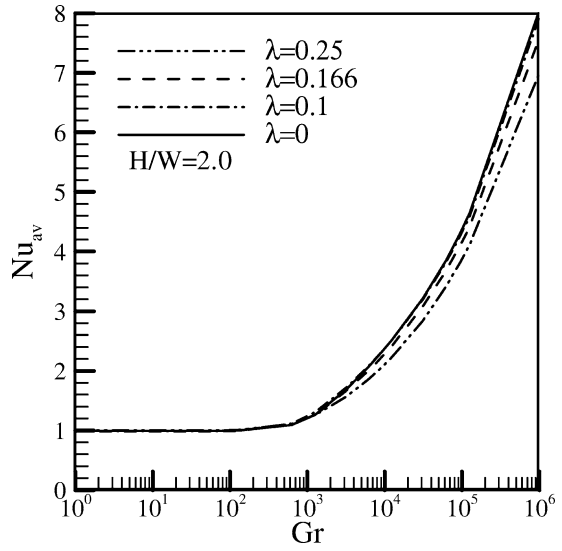

Fig. 5. Nusselt number as a function of Grashof number for $A = 2.0$.

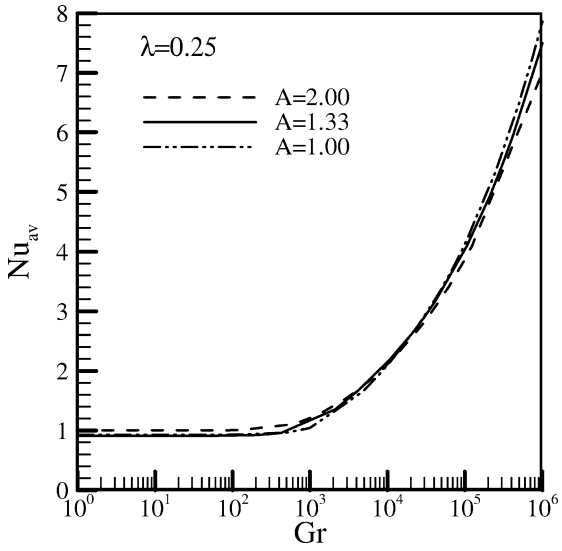

Fig. 6. Nusselt number as a function of Grashof number for $\lambda = 0.25$.

different aspect ratios $A = 2.0$, 1.33, 1.0 and a constant surface waviness $\lambda = 0.25$. Based on the Grashof number two distinct zones can be identified from the figure. For $Gr \leqslant 10^3$, the average Nusselt number is constant ($\approx$1.0) and independent of the Grashof number whatever the value of aspect ratio. This is actually the conduction regime, and in this regime heat transfer rate is mainly dominated by conduction. For $Gr \geqslant 10^3$, the Nusselt number increases and shows little influence of the aspect ratio. Magnitudes of average Nusselt number is slightly higher for lower aspect ratio.

3.3. Effect of surface waviness

Fig. 7 shows the distribution of average Nusselt number as a function of surface waviness (λ) for $A = 2.0$ and

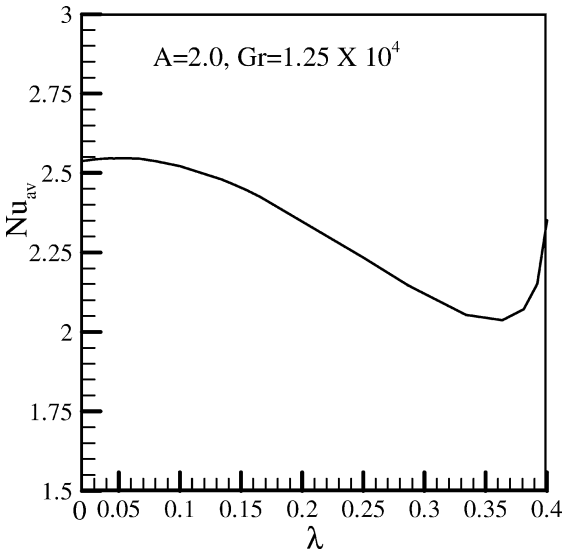

Fig. 7. Nusselt number as a function of surface waviness for $A = 2.0$ and $Gr = 1.25 \times 10^5$.

$Gr = 1.25 \times 10^4$. A very lower value of surface waviness (i.e., $\lambda \leqslant 0.05$) does not play any effective role on the average heat transfer. Heat transfer is invariant with surface waviness below $\lambda \approx 0.05$. In a middle range of surface waviness (i.e., $0.05 \leqslant \lambda < 0.325$), heat transfer gradually falls with surface waviness. Closer to the value $\lambda \approx 0.325$ these scenarios again changes and for a very small range of λ ($0.325 \leqslant \lambda \leqslant 0.37$) the average heat transfer is again shows no variation with λ. Further increase of surface waviness heat transfer increases with the increase of λ. At such high waviness, interwall spacing closer to the top end becomes small causing no convective distortion of the isotherms. The local heat transfer rate (as well as Nu_L) is higher near the top end of the cavity for the higher value of surface waviness (λ). This will be easily understood from Fig. 4. For a particular Y/A, difference between the local Nusselt number is small for $Y/A \leqslant 0.85$ at different λ. For $Y/A > 0.85$, higher the value of surface waviness larger the value of Nu_L (Fig. 4). So, when integrated, Nu_L distribution for $\lambda = 0.4$ produces larger Nu_{av} than Nu_{av} at λ slightly lower than 0.4 and so on. But this type of scenario is only restricted for the surface waviness $\lambda \geqslant 0.35$.

3.4. Velocity and temperature profile

Profiles of dimensionless vertical velocity (V) and temperature (Θ) are presented in Fig. 8(a) and (b) for four selected Grashof numbers ($Gr = 10^3$, 10^4, 10^5 and 10^6), an aspect ratio $A = 2.0$ and surface waviness $\lambda = 0.25$ at $Y = 0.5$. At $Gr = 10^3$ and 10^4, velocity profiles in between the wall and vertical centerline are similar to the parabolic profiles inside two parallel plates. The velocity is higher for $Gr = 10^4$ than for $Gr = 10^3$ at every point from the centerline to the wall. A further increase of the Grashof number increases the peak velocities but now the profiles shift towards the vertical

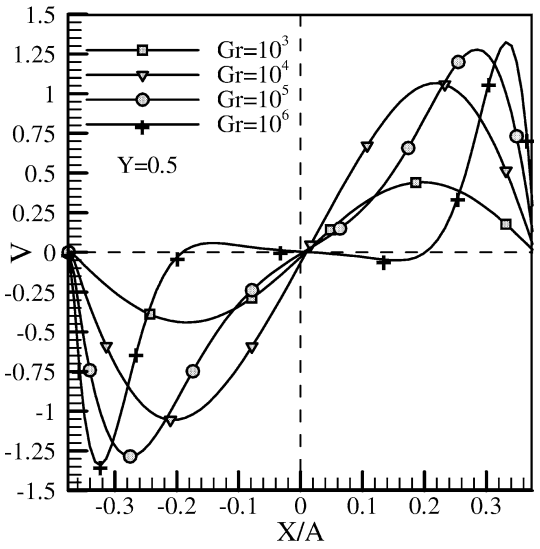

(a)

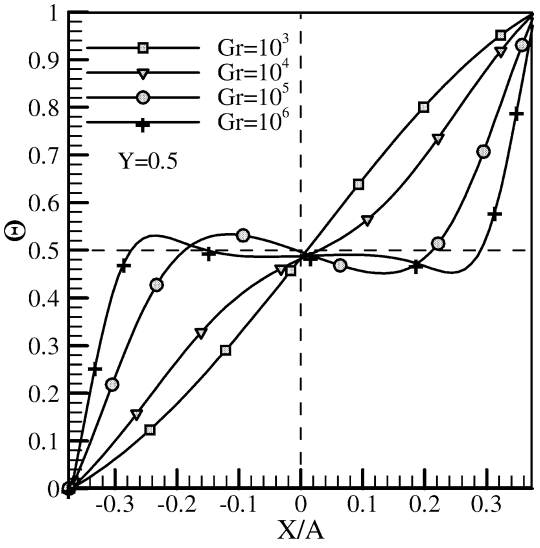

(b)

Fig. 8. (a) Vertical velocity profiles for $A = 2.0$ and $\lambda = 0.25$ at $Y = 0.5$. (b) Temperature profiles for $A = 2.0$ and $\lambda = 0.25$ at $Y = 0.5$.

walls (hot or cold wall) and are concentrated. Velocities near the center of the cavity decrease with further increase of the Grashof number. The fluid is almost motionless ($V \approx 0$) in the center.

3.5. Flow and thermal field

The flow pattern inside the cavity and the thermal field are presented in terms of streamlines and isotherms contours in Fig. 9(a)–(e) for $A = 2.0$, $\lambda = 0.25$ at six different Grashof numbers. Hot fluid moves up along the hot wall and turns to the left at the top adiabatic wall and then mixes with the fluid that moves downward along the cold wall. This creates a circulation inside the cavity, which is very weak at low Grashof number ($=10^2$). Isotherms are vertical and strongly follow the geometry (waviness along the vertical direction) of the surface at low Grashof numbers as shown in Fig. 9(a). Convection is less dominant at this Grashof number and heat transfer is mainly by conduction. The basic difference between the isotherms in a rectangular cavity and a wavy cavity at such Grashof numbers is their shape. A further increase of Grashof numbers increases the circulation inside the cavity. At $Gr = 10^3$ and 1.25×10^4, streamlines shows a similar pattern as for $Gr = 10^2$ except that the shape of the core is slightly deformed. But isotherms turn back (convective distortion) towards the cold wall due to the strong influence of the convection current. Isotherms are concentrated at the bottom of the hot wall and at the top of the cold wall. As the Grashof number increases ($Gr = 2.5 \times 10^4$) the core of the streamline starts to distort. The isotherms in Fig. 9(d) in the middle of the cavity start to become horizontal with a low temperature gradient that cause the distortion of central streamline. At $Gr = 1.25 \times 10^5$, a thermal boundary layer forms. Isotherms are highly concentrated at the wavy wall. Central isotherms are horizontal with an almost vanishing or negative temperature gradient, that causes a further distortion of the streamline core. The core is divided into two counter rotating vortices of nearly elliptic shape. At $Gr = 10^6$, isotherms shift towards and concentrated near the wavy walls causing rise of temperature gradient ($\partial\Theta/\partial X$) in the vicinity of the wavy walls. The convection between each layer leads to a negative $\partial\Theta/\partial X$ in the center of the cross-section [12] causing two secondary vortices. At $Gr = 10^6$, another vortex appears at the center of the cavity. The pair of counter rotating vortices appeared previously move further towards the wavy wall.

4. Conclusion

Heat transfer characteristics with flow structure are studied numerically in this paper for a cavity with differentially heated vertical wavy walls. The effect of aspect ratio, surface waviness on heat transfer is tested at different Grashof numbers. Higher heat transfer is observed at lower aspect ratios for a certain value of the Grashof number, above which heat transfer shows little variation whatever the aspect ratio be. This depends strongly on the surface waviness. For a particular aspect ratio, heat transfer is constant and independent of the Grashof number. This conduction regime is determined by certain range of Gr. Above this range, heat transfer increases with the increase of Grashof number. The lower the surface waviness, the higher is the heat transfer. For a constant Grashof number and aspect ratio, heat transfer falls gradually with an increase of surface waviness up to a certain value of surface waviness, above which heat transfer increases again.

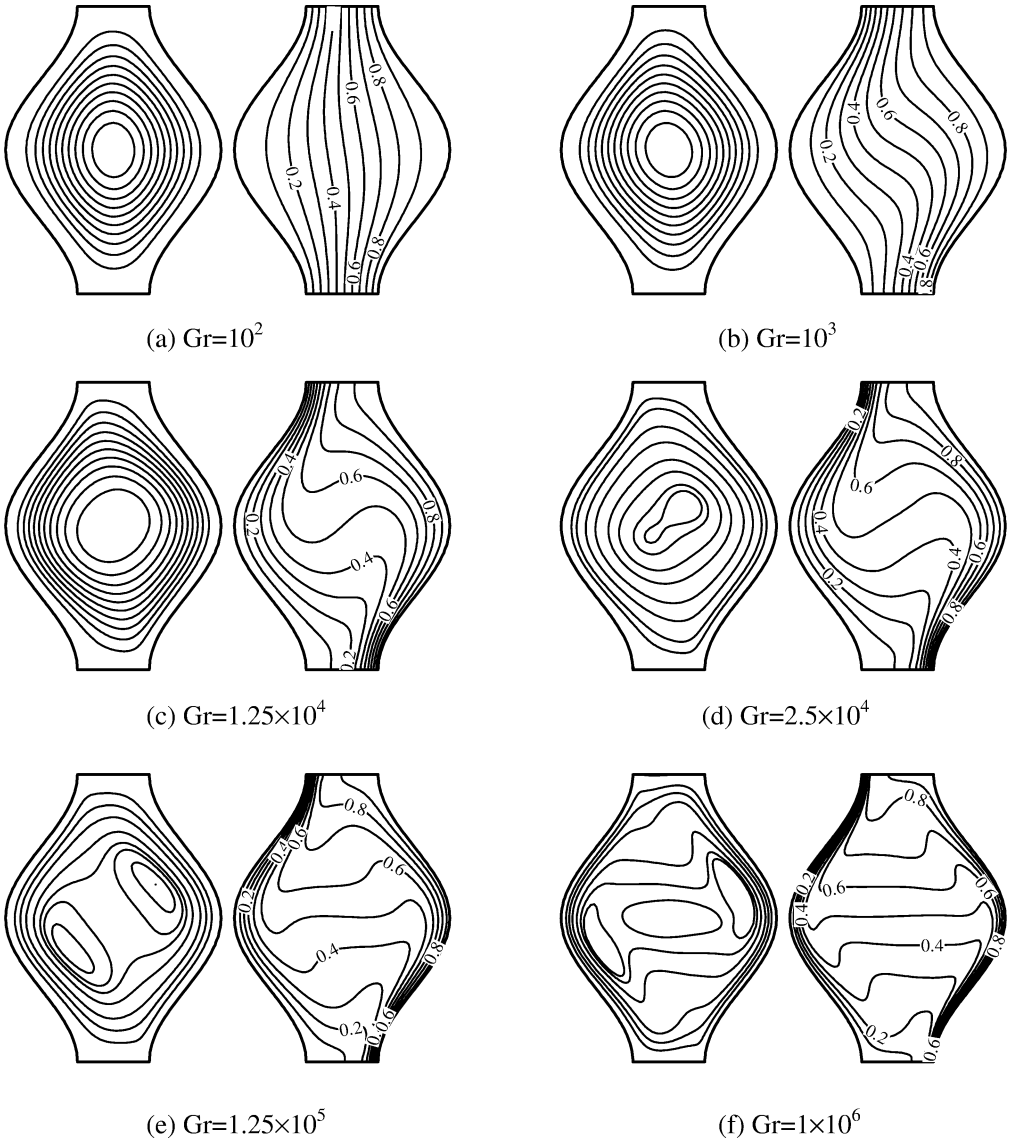

Fig. 9. Streamlines (left) and isothermal lines (right) for $A = 2.0$ and $\lambda = 0.25$ for (a) $Gr = 10^2$, (b) $Gr = 10^3$, (c) $Gr = 1.25 \times 10^4$, (d) $Gr = 2.5 \times 10^4$, (e) $Gr = 1.25 \times 10^5$, (f) $Gr = 10^6$.

References

[1] A. Hadjadj, M.E. Kyal, Effect of two sinusoidal protuberances on natural convection in a vertical annulus, Numer. Heat Transfer A 36 (1999) 273–289.

[2] B.V.R. Kumar, A study of free convection induced by a vertical wavy surface with heat flux in a porous enclosure, Numer. Heat Transfer A 37 (2000) 493–510.

[3] L.S. Yao, Natural convection along a vertical wavy surface, J. Heat Transfer 105 (1983) 465–468.

[4] C. Saidi, F. Legay, B. Pruent, Laminar flow past a sinusoidal cavity, Internat. J. Heat Mass Transfer 30 (1987) 649–660.

[5] Y. Asako, M. Faghri, Finite volume solution for laminar flow and heat transfer in a corrugated duct, ASME J. Heat Transfer 109 (1987) 627–634.

[6] J.L. Lage, A. Bejan, Convection from a periodically stretching plane wall, J. Heat Transfer 112 (1990) 92–99.

[7] F.J. Hamady, J.R. Lloyd, H.Q. Yang, K.T. Yang, Study of local natural convection heat transfer in an inclined enclosure, Internat. J. Heat Mass Transfer 32 (1989) 1697–1708.

[8] H. Ozoe, H. Sayma, S.W. Churchill, Natural convection in an inclined rectangular channel at various aspect ratios and angles—experimental measurements, Internat. J. Heat Mass Transfer 18 (1975) 1425–1431.

[9] M. Hortmann, M. Peric, G. Scheuerer, Finite volume multigrid prediction of laminar natural convection: Bench–Mark solutions, Internat. J. Numer. Methods Fluids 11 (1990) 189–207.

[10] J. Ferziger, M. Peric, Computational Methods for Fluid Dynamics, Springer-Verlag, Berlin, 1996.

[11] N.C. Markatos, K.A. Pericleous, Laminar and turbulent natural convection in an enclosed cavity, Internat. J. Heat Mass Transfer 27 (1984) 755–772.

[12] G.D. Mallinson, G.D.V. Davis, Three-dimensional natural convection in a box: A numerical study, J. Fluid Mech. 83 (1977) 1–31.